Research article

Investigating the electron tunneling effect on photovoltaic performance of almond (*Prunus dulcis*) dye-sensitized solar cell

T.J. Abodunrin [a,*], O.O. Ajayi [b], M.E. Emetere [a], A.P.I. Popoola [c], U.O. Uyor [e], O. Popoola [d]

[a] *Department of Physics, Covenant University, Ota, Nigeria*
[b] *Department of Mechanical Engineering, Covenant University, Ota, Nigeria*
[c] *Department of Chemical, Metallurgical and Materials Engineering, Tshwane University of Technology, Pretoria, South Africa*
[d] *Centre for Energy and Electric Power, Tshwane University of Technology, Pretoria, South Africa*
[e] *Department of Electrical Engineering, University of Nigeria, Nzukka, Nigeria*

A B S T R A C T

Dye-sensitized solar cells (DSSCs) are characterized by several special attributes such as low cost, ease of fabrication, all year availability of sunlight, and capacity to operate under diffuse lighting conditions. However, their universal adoption is still restricted by a low efficiency photovoltaic output. Thus, this research seeks to explore avenues of present photon mitigation which could be corrected in future DSSC technology in order to improve on existing efficiency records. A preliminary phytochemical screening of *Prunus dulcis* (*P. dulcis*) leaf extract revealed a variety of chromophores which renders high possibility for charge transport. UV/VIS spectroscopy showed *P. dulcis* with peak absorbance wavelength within the visible region of the electromagnetic spectrum of light. Fourier transform infrared spectroscopy specifically highlighted the fingerprint of the chromophores present in this organic extract. Photovoltaic parameters such as short circuit current (I_{sc}), open circuit voltage (V_{oc}), maximum power (P_{max}), fill factor (*ff*) and efficiency (η) were the factors taken into consideration for the determination of the photovoltaic outcome. In *P. dulcis* DSSCs, KBr electrolyte recorded the best η of 10.18%. However, *P. dulcis* DSSC with electrolyte KI indicated the best I_{sc}, V_{oc} and P_{max} of 0.135 mA, 280 mV and 34.2 mW respectively. The similarity of this photovoltaic result with previous DSSC results necessitated further analysis. Consequently, scanning electron micrograph (SEM) of *P. dulcis* was modelled first with Gwyddion software and this output was analyzed with Excel and Origin programs. The outcome is a scientific discovery of electron tunneling in the *P. dulcis* shells, effect of dopant ions boosting the electrolytic Fermi level and a high probability of influencing the future efficiency outcome in *P. dulcis* DSSCs. Using mathematical algorithms from the Origin and Excel software applications, a direct function of the impact of doping, relative speed of electrolyte molecules as they percolate *P. dulcis* framework was obtained. Thus, the significance of this work lies in the relationship of behavioral dynamics of dopants to photovoltaic performance of *P. dulcis*. This indicates that a vital optical tunable characteristic of DSSCs lies in electrodynamics of dopant ions, which presents a viable prospect for application in DSSC technology research.

1. Introduction

Charge transport can be viewed from the dual perspective of wave-particle theory. It generally postulates that, when photons of appropriate frequency impinge on the dye-sensitized solar cell device, photo excited electrons travel in a conduit [1]. In this wave-particle context, charge transport is a complex phenomenon explained by quantum tunneling, because its pattern is not straightforward, it cannot be directly observed [2]. Moreover, a great deal of knowledge of what happens on

the microscopic level is not sufficiently classified in classical mechanics [3]. To gain greater insight into this phenomenon, a second perspective, the concept of electrons behaving like particles which are obstructed by potential barriers, is therefore fundamental in simplifying the disparity between classical and quantum mechanics outlook [4]. In general terms, classical scientists base their calculation on electron particles lacking adequate energy to overcome the obstacles along their path. They attribute this to the occurrence of reflection or absorption in extreme cases [5]. Whereas, quantum mechanics considers a little probability that the

---

electron successfully tunnels through certain barriers despite the resistances [6]. The energy in this case, is accounted for by the electron acquiring energy supply from its environment [7]. This in turn, offers the study of probability on how far the electron transits, from the valence to conduction band. Since energy is in form of discrete pockets, the wave nature comes to the fore [8]. In the recent past, Schrödinger wave functions have been used extensively to predict the electron tunneling in nanocomposites [9]. This however, introduces another measure of uncertainty. Although the wave function of the electron particle sums up the facts about any physical system, this probability wave function is directly associated with the density of the particle's position, creating a possibility that the particle is at that given point within a time reference. Inside the boundary of large barriers, probability of tunneling decreases for higher and broader barriers [10]. In order to reduce these ambiguities, simple tunneling-barrier models were considered, the outcome was a logical solution that is still regularly used for prediction. Real-life situations such as those presented by dye-sensitized solar cells often do not have only one unique solution. Thus, the classical or quasi-classical approaches are used to give estimated answers to these problems. Therefore, although probabilities may be derived from chance accuracy, the solution or roots require constraint by computational resources [11]. In addition, several researches have considered the effect of designing products, processes and production systems that can be easily scaled-up. This forms the basis for a sustainable development, some studies delved into trapping a suitable liquid electrolyte in polymer electrolyte membranes as a means of improving long-term stability. In this context, researches focused on obtaining high-level long-term performance through consideration of components utilized for energy conversion and storage devices. The outcome was functionalized and biodegradable end-products which stand out and find viable application in Lithium batteries, super capacitors and hydrogen gas production [12]. Thus, this research work would use Gwyddion, Excel and Origin program to interpret the spectroscopy results obtained from the experiment on *P. dulcis* DSSCs. This in turn would be used to explain the effect of electron tunneling on *P. dulcis* photovoltaic performance with a focus on future application in optoelectronics.

2. Materials and method

2.1. Dye extraction

P.dulcis organic dye was obtained from stoichiometric amount of *P. dulcis* leaves harvested from a tree. 4.0 kg of the leaf part was collected and weighed with an electronic balance. This leaf sample was laboratory dried until it became constant in weight. After this procedure, the dried leaf was grinded to a coarse mass which was then spread out to allow unwanted moisture and vapors condense out. After sufficient hours for cooling down to room temperature, the cool leaf sample was totally soaked in 50 ml of methanol of commercial variety inside thin layer chromatography tanks. The choice of solvent was purely based on previous scientific record of high yield [13]. The set-up was allowed to remain for 264 h to extract sufficient *P. dulcis* dye. The final step was pouring the methanolic mixture through sterilized filters to collect *P. dulcis* filtrate in reagent bottles. The *P. dulcis* dye was obtained from rotary evaporator set ambiently at 226 revolutions per minute to preserve the chromophores. The pH of *P. dulcis* was 5.49 with an ambient temperature of 27.1 °C.

2.2. Preliminary screening

The following laboratory tests were carried out on 1g of *P. dulcis* dissolved in 100 ml of distilled water (DW) according to standard procedure [14]. A test was adjudged positive when distinctive colour change confirmed the presence of particular chromophores which aided the charge transport. A greenish-black precipitate indicated that tannin was present when 2 ml of 5% ferric chloride was added in 1 ml of dye extract.

Formation of a sheet of persistent layer of bubbles showed that saponin was present when 2 ml of distilled water (DW) was added to 2 ml of the dye extract and vigorously shaken for about 0.25 h. A yellow colour confirmed that flavonoid was present when 5 ml of dilute ammonia solution was added to 2 ml of dye extract and three drops of concentrated H_2SO_4.In addition, presence of a brown ring at an interface showed the presence of cardiac glycosides as two drops of 5% ferric chloride solution mixed with 2 ml of glacial acetic acid was added to 0.5 ml of dye extract. Also, a green colour indicated that alkaloid was present when 2 ml of DW was added to 1 ml of dye extract, followed by a few drops of 10% ferric chloride then, concentrated H_2SO_4 was carefully added as a layer under the already existing mixture. Finally, a green coloration indicated the presence of phenol when 2 ml of concentrated HCl was added to 2 ml of the dye extract and two drops of Mayer's reagent was introduced inside the solution. 0.1 g of *P. dulcis* dye extract was dissolved in 100 ml methanol to obtain the UV/VIS and FTIR spectrograph from Thermo-scientific Evolution 60S series UV/VIS and Shimadzu IR spectrophotometer respectively [15].

2.3. Fabrication of P. dulcis DSSC

Four sets of indium doped tin-oxide (ITO) conducting glass comprising of a pair each, were tested for their conducting slide with a multimeter and labelled accordingly. An active area of (2.41 cm × 1.31 cm), 3.16 cm^2 was marked off with masking tape for consequent exposure to radiation. The photoanode preparation consisted of a colloidal blend of concentrated HNO_3 and titanium oxide of commercial variety. This mixture was consequently applied onto the conducting side via the doctor blade method technique and sintered [14, 15]. The customary colour change of cream–brown-cream was affirmation that the photoanode was ready for use. *P. dulcis* dye was then grown on the photoanode surface by capillary action for further use. The counter electrode was prepared by coating the second pair of ITO with epitaxial layer of soot from a naked Bunsen flame in a simulated vacuum enclave. The two slides were then fastened with strong binder clips and injected with two drops of electrolytic solution of electrolyte. The electrolytes used were KCl, KBr, KI and $HgCl_2$ constituted from 1 g of their solute dissolved in 100 g of distilled water. Each DSSC was then connected in parallel with a variable resistor and Multimeter to obtain readings under 1.5 air mass conditions.

3. Results and discussion

3.1. Phytochemical analysis

The qualitative phytochemical screening procedures revealed the presence of several functional groups such as, tannin, saponin, flavonoid, alkaloid, cardiac glycoside and phenol.

P. dulcis records peak absorbance within the visible region of the electromagnetic spectrum as shown in Figure 1. The significance of this result according to Beer Lambert's law [16] is as shown in Eqs. (1) and (2):
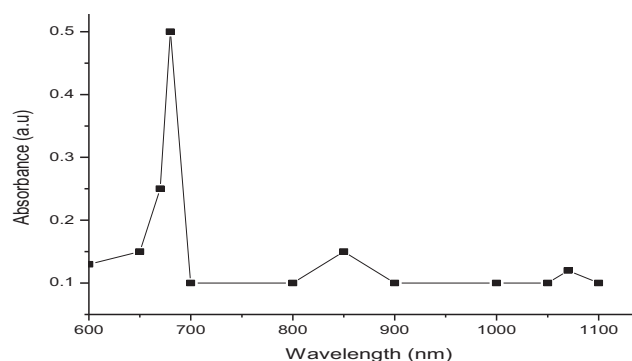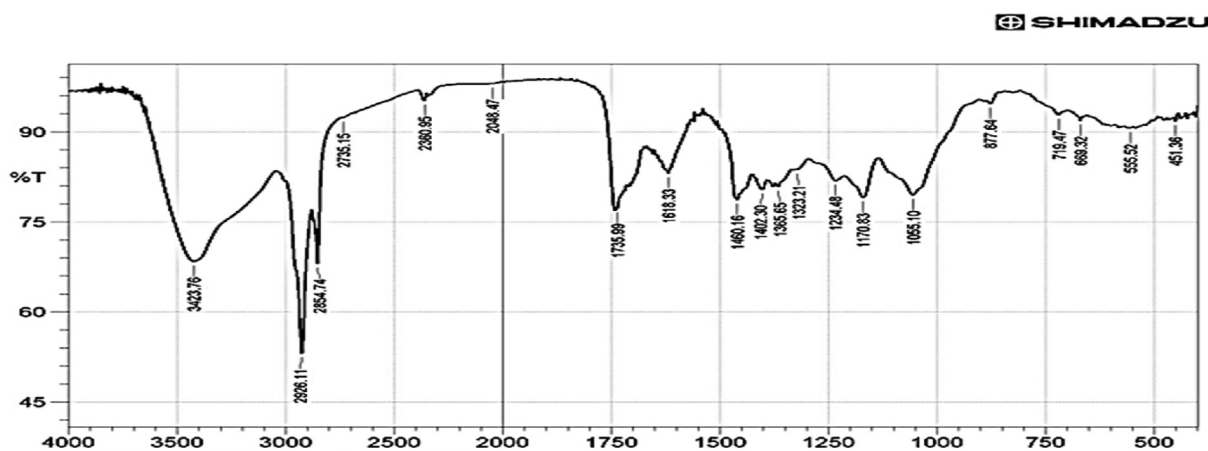

Figure 1. UV/VIS of *P. dulcis* dye.

Figure 2. *P. dulcis* FTIR Spectrograph.

Table 1. FTIR of *P. dulcis* dye.

P. dulcis dye	Absorption Peak (cm)$^{-1}$	Type of bond
	555.52 *s*	C–Br
	1055.10 *s*	C-OOR stretch
	1170.83 *m*	C–H wag
	1365.65 *m*	C–H rock
	1460.16 *m*	Aromatic C–C stretch
	1618.33 *m*	C=O aromatic
	1735.99 *s*	C=O stretch
	2854.74 *s*	}C–H (aliphatic)
	2926.11 *s*	
	3423.76 *v*	O–H stretch

Key: *s*-strong, *m*-medium, *v*-varies.

$$A = \varepsilon c l \tag{1}$$

where A is the absorbance (a.u), ε is molar extinction coefficient (mol/dm^3), c is the concentration of the dye and l is the length of the cuvette (cm).

In this study, $A_{\lambda(670)} = -\log T \tag{2}$

where T is the transmittance of dye in %, λ is the wavelength in nm. The significance of this wavelength is that *P. dulcis* dye would be perceived as brownish red within the visible range, this implies that *P. dulcis* dye has a long wavelength of 660 nm and low frequency molecules. The relationship between frequency and wavelength is described as,

$$\nu = f \lambda \tag{3}$$

where *v, f* and λ represent velocity (m/s), *f* is the frequency (Hz) and λ is the wavelength (in nm).
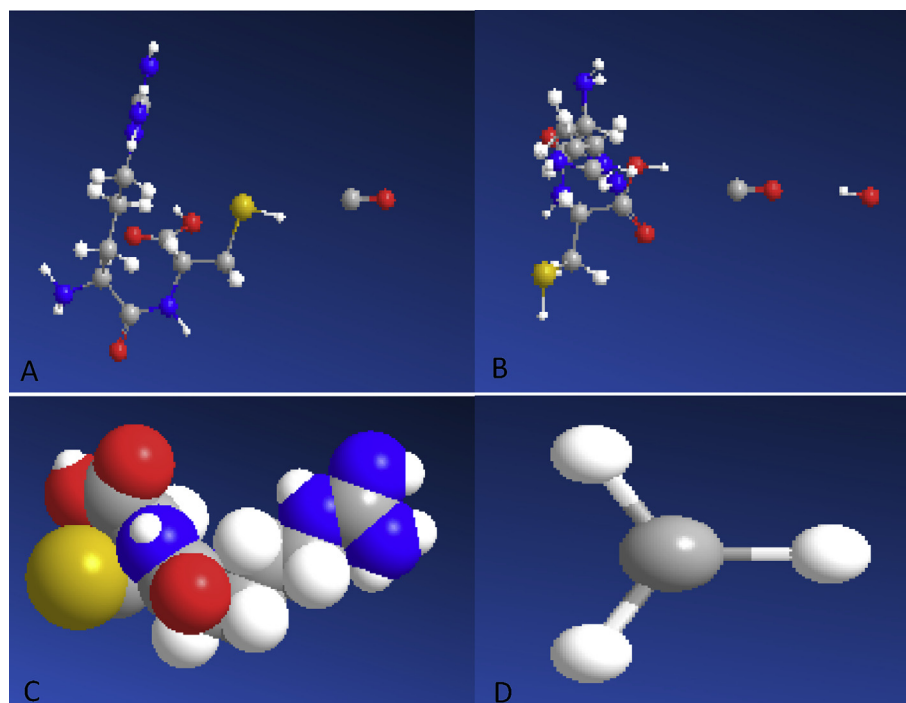
Figure 3. Molecular Structural Representation of *P. dulcis* dye's FTIR spectrograph in (a) C=O and (b) O–H auxochrome, (c) –COOR and (d) –CH chromophore.
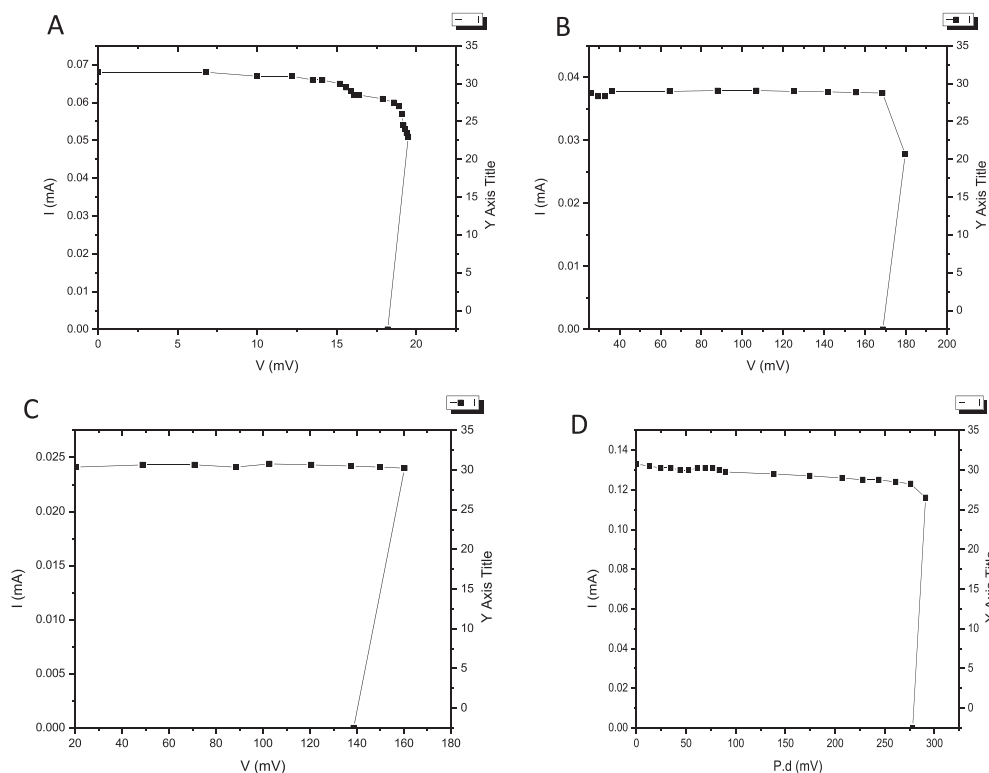
Figure 4. Photovoltaic responses of *P. dulcis* DSSC with (a) KCl (b) KBr (c) HgCl$_2$ and (d) KI.

Table 2. Photovoltaic performance of *P. dulcis* DSSCs.

Photovoltaic Properties	KCl	KBr	HgCl$_2$	KI
I$_{sc}$ (mA)	0.068	0.038	0.024	0.135
V$_{oc}$ (mV)	18.00	170.0	140.0	280.0
P$_{max}$ (mW)	0.065	6.188	3.600	34.20
ff	0.05	0.97	1.07	0.90
η (%)	0.02	1.96	1.14	10.18

The fill factor (*ff*) for *P. dulcis* DSSC sensitized with HgCl$_2$ electrolyte exceeds the standard limit, 1. This is attributable to variations arising from computation in designated significant figures.

By calculation, v is $3 \times 10^8 m/s$ and λ is 0.66 m then f is $45 \times 10^6 / s$ which is low relative to ultraviolet radiation which has high frequency and short wavelength.

3.2. FTIR Spectroscopy analysis

The infrared spectrograph presents the functional chemical groups in *P. dulcis* dye. Figure 2 is the pictorial illustration of the electron withdrawing and electron donating reactions. Table 1 further clarifies the particular nature of transfer which occurs. Therefore, Figure 3(a) and (b) describe the electron donating auxochromates as they articulate with other atoms. Figure 3(c) shows chromophores of *P. dulcis* dye and the manner they connect in a conjugated system. The importance of the mode *P. dulcis* bonds with other molecules brings to bear a hypothesis, that *P. dulcis* is not ruthenium in nature, the nucleated center is not typical of ruthenium atom's interface with different atoms, neither is it porphyrin as depicted by the UV/VIS characteristic absorbance.

3.3. Photovoltaic characterization of P. dulcis DSSC

Spectral responses of *P. dulcis* DSSCs current – voltage properties elicited is as shown in Figure 4, this remains a valid parameter for assessing the class of a dye. However, it is pertinent to consider the other photovoltaic metrics that contributed to the overall efficiency as shown in Table 2. The most efficient electrolyte with *P. dulcis* dye is KBr, while the least efficient electrolyte is KCl as illustrated in Figure 4(a) and (b) respectively. This is attributable to good charge transport and minimal recombination, which electron tunneling promotes. Conversely, the highest V$_{oc}$ was recorded in *P. dulcis*/KI as shown in Figure 4(d). This suggests that, the Fermi level of I$^-$ is less than the other ions causing it to require less energy for I$^-$ to be excited and preferentially discharged. The difference in V$_{oc}$ is almost 65% between KBr and KI. The largest I$_{sc}$ was recorded with KI electrolyte while the least was observed in *P. dulcis*/HgCl$_2$ as shown in Figure 4(c). Thus, electron tunneling was highest with KCl probably due to high recombination of Cl$^-$ and electron tunneling was least with KI due to favorable kinematics of reaction with I$^-$. This is probably due to *P. dulcis*/KI's outstanding *ff* which describes a very high quality DSSC. The highest P$_{max}$ was observed in *P. dulcis*/KI electrolyte, this buttresses the preferential discharge of I$^-$. Ultimately, this result collaborates with previous result from researches from similar research work. The output efficiency lies within the range of 0.02 and 10.18% as shown in Table 2. These results show high probability that the earlier hypothesis leads to *P. dulcis* dye as a triphenylamine dye, which is utilized for its optoelectronic properties in DSSC applications. The low efficiency output of DSSCs is therefore a direct mitigation of electron tunneling which results in electron-hole recombination, unnecessary heat and unfavorable chemical kinematics of redox reactions. The η and *ff* were determined by calculation from Eqs. (4) and (5) [5, 17].
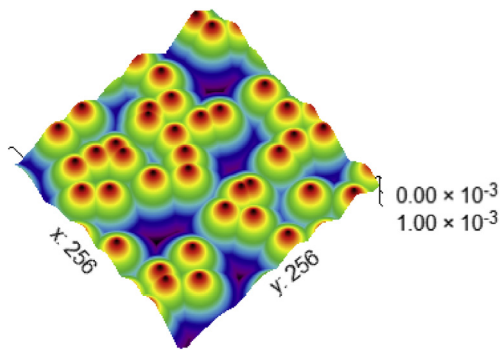
Figure 5. Gwyddion plot of *P. dulcis* dye.

$$\eta = \frac{I_{SC}\ V_{OC}*ff}{A*G} \qquad (4)$$

$$ff = \frac{P_{max}}{I_{Sc}V_{OC}} \qquad (5)$$

where I_{sc}, V_{oc}, ff, A, G and P_{max} represent short circuit current (mA), open circuit voltage (mV), fill factor, active area of DSSC, power of irradiance and maximum power (μW).

Thus, from Eqs. (4) and (5), $\eta_{kcl} = \frac{0.065}{3.16*100}*100 = 0.02\%$ This was applied for all the electrolytes to obtain the parameters presented in Table 2.

3.4. Gwyddion investigation of electron tunneling in P.dulcis dye

Knowledge of *P. dulcis* dye microstructure is crucial to justify the photovoltaic output of *P. dulcis* DSSCs. The red dots in Figure 5 represent the electron shells in *P. dulcis* dye. A close inquiry of the Gwyddion plot reveals that few electrons occupy the lower shell. The larger percentage of the electrons are clustered in the middle region. The implication of this is that, if the Fermi energy acquired by the *P. dulcis* atoms either from the electrolytes or photons is sufficiently high enough, they would transit to the higher valence band. On the other hand, if the energy supplied is not adequate, more electrons would drop to the lower energy valence band. The blue region depicts areas for electron tunneling. This section cordons the electron shells in the middle of the figure from the few electrons in the valence band. Thus, the probability of electron diffusion or hopping is the only method of populating the higher electron shell. Electron tunneling would demand a higher fermi level with a possible risk of recombination. The significance of this inquiry is therefore to promote the preferentially discharged Br^- or I^- ions. Application of nanowires or arrays would create a measure of stability and thereby improve on
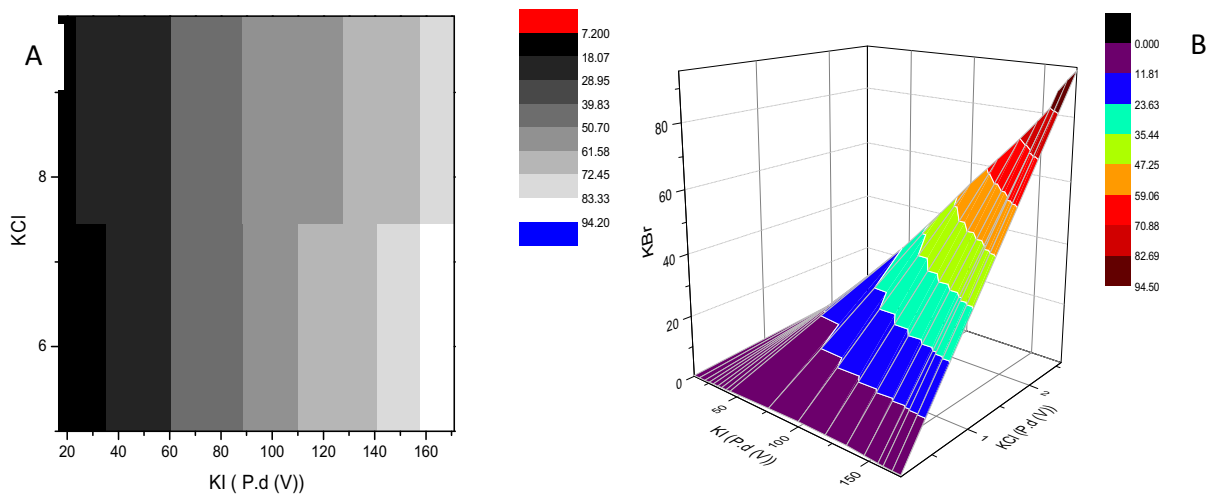

Figure 6. Electrodynamics of *P. dulcis* showing (a) infiltration of ions and (b) comparison of P. d in reference different ions.
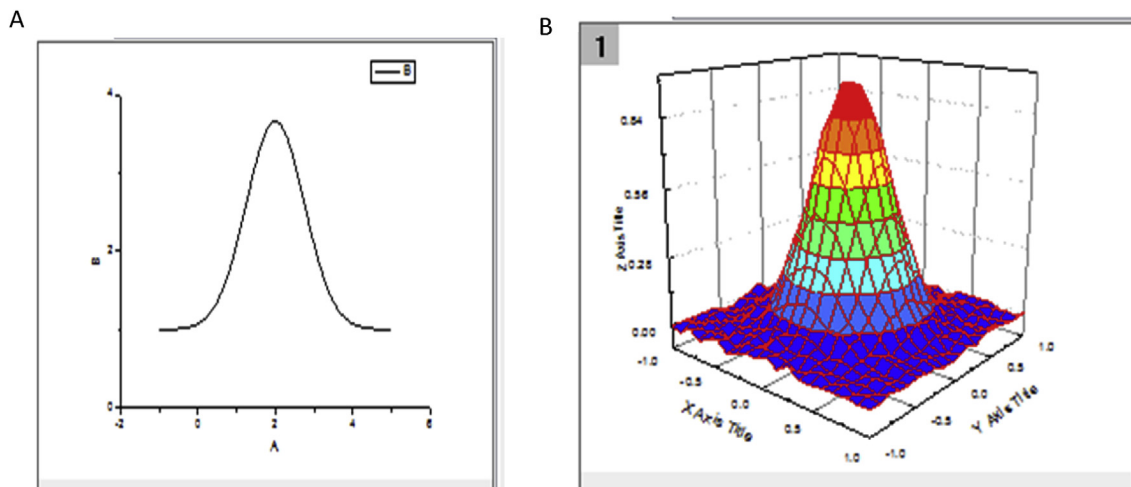

Figure 7. (a): Gaussian function of the power density of dopants during electron tunneling in *P. dulcis* and (b) Specified surface function using Gauss 2D function.
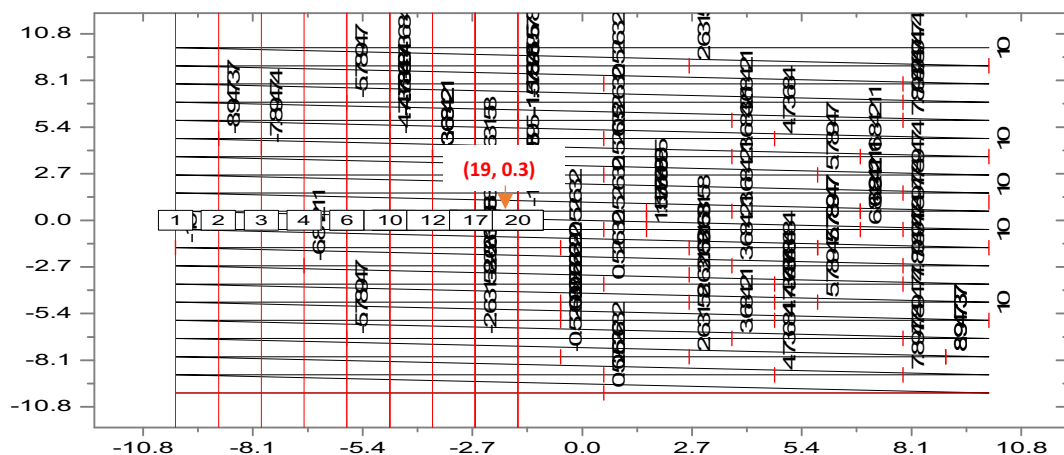
Figure 8. Peak analyzing of *P. dulcis* DSSCs.

charge transport similar to that obtained in Ruthenium complexes and push-pull porphyrin dyes [17].

3.5. Electrodynamics of charge transport in P. dulcis DSSCs

The Origin software was used to analyze the I–V curves more intricately, Cl^- ions percolated 27 units on a scale of 170 while, I^- ions infiltrated excellently with a distinctive V_{oc} as illustrated on Figure 6(a). A comparative analysis of three electrolytes is shown in Figure 6(b). KCl connotes the baseline depicted in black and purple hue, the peak depicted by toffee brown shows the penetration and possible relative speeds of Br^- ions. I^- are represented by the red colour.

A deeper probe of the impact of the penetration of electrolytic dopants into *P. dulcis* dye frame was analyzed using the Gauss function. The power density of dopants is revealed by the success of transport for each DSSC is shown in Figure 7(a). Differentiation using specified surface function gives a better picture in Figure 7(b). Cl^- ions occupy the base area of the power density function, the purple colour depicts the Cl^- domain, a gradual transition all the way to sky blue represents an inter mingle from $HgCl_2$ electrolyte ions. The lime green introduces the KI electrolyte terrain, an intermission again where a peak is shown by the yellow colour. The infusion climaxes with the red peak signifying the Br-ions. Although, the colour code used is arbitrary, the colour of the margins are undisputedly direct representation of the original values. This interprets a converse wherein charge transport occurs without the inhibitive electron tunneling.

A peak analyzer was used to further analyze the dopant concentration, the effect is displayed in Figure 8. The numbers reflect a region of densely packed dopants ions which translate to better charge transport and a higher photovoltaic output. The co-ordinates of translation occur when the anchor is at (19, 0.3).

4. Conclusion and recommendation

This research proved the hypothesis that open circuit voltage in dye-sensitized solar cells is a direct function of electrolytic ion percolation inside the photoanode molecular structure. It offers a unique micro structural perspective on solving the challenges of dire limitation to the application of all thin film solar cells. Electron tunneling investigation as one of the preliminary examinations thus, provides an archetypical model for more efficient dye-sensitized solar cell technology in future inquiries. Provision of an efficient conduit for charge transport like nano-meshes would reduce the effect of electron tunneling, increase the speed of electron and eliminate recombination time in the blue domain considerably. This corroborates the photovoltaic outcome in this study, KI electrolyte recorded the best V_{oc} and consequently, the highest η. The least V_{oc} was recorded in KCl with the poorest η. In effect, KBr and $HgCl_2$

electrolytes also validate the direct impact of electron tunneling on V_{oc}. A limitation to this study lies in the scope or percentage measure of electron tunneling factor which occurred in *P. dulcis* DSSC.

References

[1] W.J. Lee, E. Ramasamy, D.Y. Lee, J.S. Song, Dye-sensitized solar cells: scale up and current-voltage characterization, Sol. Energy Mater. Sol. Cells 91 (2007) 1676–1680.

[2] M.A. Hasan, K. Sumathy, Photovoltaic thermal module concepts and their performance analysis: a review, Renew. Sustain. Energy Rev. 14 (7) (2010) 1845–1859.

[3] H. Hoppe, N.S. Sariciftci, Organic solar cells: an overview, J. Mater. Res. 19 (7) (2004) 1924–1945.

[4] E. Stathatos, Dye sensitized solar cells: a new prospective to the solar to electrical energy conversion. issues to be solved for efficient energy harvesting, Eng. Sci. Technol. Rev. 5 (2012) 9–13.

[5] D. Joly, L. Pellejà, S. Narbey, F. Oswald, J. Chiron, J.N. Clifford, E. Palomares, R. Demadrille, A robust organic dye for dye sensitized solar cells based on iodine/iodide electrolytes combining high efficiency and outstanding stability, Sci. Rep. 4 (2014) 4033.

[6] H.M. Upadhyaya, S. Senthilarasu, M. Hsu, D.K. Kumar, Solar energy materials & solar cells Recent progress and the status of dye-sensitised solar cell (DSSC) technology with state-of-the-art conversion efficiencies, Sol. Energy Mater. Sol. Cells 119 (2013) 291–295.

[7] T. Chen, R. Ishihara, K. Beenakker, Hot carrier effect and tunneling effect of location- and orientation-controlled (100)- and (110)-oriented single-grain si tfts without seed substrate, IEEE Trans. Electron Devices 58 (1) (2011) 216–223.

[8] R. Soltani, A.A. Katbab, The role of interfacial compatibilizer in controlling the electrical conductivity and piezoresistive behavior of the nanocomposites based on RTV silicone rubber/graphite nanosheets, Sens. Actuators, A 163 (2010) 213–219.

[9] W. Li, A. Dichiara, J. Bai, Carbon nanotube-graphene nano-platelet hybrids as high-performance multifunctional reinforcements in epoxy composites, Compos. Sci. Technol. 74 (2013) 221–227.

[10] Y. Yu, S. Song, Z. Bu, X. Gu, G. Song, L. Sun, Influence of filler waviness and aspect ratio on the percolation threshold of carbon nanomaterials reinforced polymer nanocomposites, J. Mater. Sci. 48 (2013) 5727–5732.

[11] I. Balberg, D. Azulay, Y. Goldstein, J. Jedrzejewski, G. Ravid, E. Savir, The percolation staircase model and its manifestation in composite materials, Eur. Phys. J. B 86 (2013) 1–17.

[12] F. Bella, A. Chiappone, J. Nair, G. Meligrana, C. Gerbald, Novel cellulose-based composite polymer electrolytes for green, efficient and durable energy conversion and storage devices, Chemical Eng. Trans. 41 (2014) 211–216.

[13] W.S. Bao, S.A. Meguid, Z.H. Zhu, G.J. Weng, Tunneling resistance and its effect on the electrical conductivity of carbon nanotube nanocomposites, J. Appl. Phys. 111 (2012), 093726:1–093726:7.

[14] T.J. Abodunrin, A.O. Boyo, M.R. Usikalu, M.E. Emetere, O.O. Ajayi, C. Kotsedi, Z.Y. Nuru, M. Malik, G. Oghonyo, Influence of n-Mosfet transistor on dye-sensitized solar cell efficiency, Heliyon 4 (12) (2018), e01078.

[15] T.J. Abodunrin, M.E. Emetere, O.O. Ajayi, A.P.I. Popoola, U.O. Uyor, O. Popoola, Investigating the prospect of micro-energy generation in *S.Anisatum* Dye-sensitized solar cells (DSSCs), IOP Conf. Series (2019) 1299.

[16] O. İçelli, Z. Yalçin, The spectral applications of Beer-Lambert law for some biological and dosimetric materials, AIP Conf. Proc. 1611 (2014) 199.

[17] W. Xu, B. Peng, J. Chen, M. Liang, F. Cai, New triphenylamine-based dyes for dye-sensitized solar cells, J. Phys. Chem. C (2008) 1123874–1123880.